Heliyon 6 (2020) e04590

Contents lists available at ScienceDirect

Heliyon

journal homepage: www.cell.com/heliyon

Research article

Polyurethane film prepared from ball-milled algal polyol particle and activated carbon filler for NH_3–N removal

Marlina [a,*], Muhammad Iqhrammullah [b], Sitti Saleha [a], Fathurrahmi [a], Fandini Putri Maulina [a], Rinaldi Idroes [a,c]

[a] Department of Chemistry, Faculty of Mathematics and Natural Sciences, Universitas Syiah Kuala, Kopelma Darussalam, Banda Aceh 23111, Indonesia
[b] Graduate School of Mathematics and Applied Sciences, Universitas Syiah Kuala, Kopelma Darussalam, Banda Aceh 23111, Indonesia
[c] Department of Pharmacy, Faculty of Mathematics and Natural Sciences, Universitas Syiah Kuala, Kopelma Darussalam, Banda Aceh 23111, Indonesia

ARTICLE INFO

Keywords:
Algae
NH3–N adsorption
Polyurethane
Biopolyol
Activated carbon
Isotherm
Materials characterization
Water treatment
Polymerization
Adsorption
Wastewater management
Materials science
Environmental science

ABSTRACT

This research offers a novel approach of free chemical preparation to obtain algae-based biopolyol through a ball milling method. The algae-based polyurethane (AlgPU) film was obtained from a casting solution made of ball-milled algal polyol particle and methylene diphenyl diisocyanate (MDI). The characteristics of the material had been investigated using Fourier Transform Infrared, Scanning Electron Microscopy – Electron Dispersive Spectroscopy, Differential Scanning Calorimetry, and Tensile Strength Analysis. The surface area was determined by Brunauer–Emmett–Teller (BET) isotherm, meanwhile the total pore volume was by Barrett-Joyner-Halenda (BJH) isotherm, based on the adsorption-desorption of N_2. The addition of activated carbon contributed in the increase of functional group and surface area, which were important for the NH_3–N removal. As a result, the adsorption capacity increased greatly after the addition of activated carbon (from 187.84 to 393.43 μg/g). The results also suggested AlgPU as a good matrix for immobilizing activated carbon filler. The adsorption shows a better fit with Langmuir isotherm model, with $R^2 = 0.97487$ and root-mean-square error (RMSE) = 33.91952, compared to Freundlich isotherm model ($R^2 = 0.96477$ and RMSE = 44.05388). This means the NH_3–N adsorption followed the assumption of homogenous and monolayer adsorption, in which the maximum adsorption was found to be 797.95 μg/g. This research suggests the potential of newly developed material for NH_3–N removal.

1. Introduction

Indonesia has been heavily dependent on its aquaculture industries, especially in fish and shrimp production. By 2014, Indonesia had 4,000 tons/year production, becoming one of the top three aquaculture production countries in Asia, other than China and India (45,469 and 4,881 tons/year, respectively) [1]. The main challenge of keeping up this productivity is controlling the nitrogen ammonia (NH_3–N) level. This pollutant is originated from the protein-rich feed, which eventually lead to the excretion of NH_3–N from protein metabolism. Excessive NH_3–N results in various growth problems for both fish and shrimp that adversely affect the production [2, 3, 4, 5]. NH_3–N can be converted into more toxic nitrogen nitrate NO_3–N by microbes, worsening its effect on fish [6]. Additionally, NH_3–N also exacerbates an algal bloom (including *Chaetomorpha Linum*), which at the end, leads to another accumulation of NH_3–N due to the decomposition of organic matters of collapsing algae [7]. Moreover, *Chaetomorpha Linum* is considered as a dispensable solid waste of the fish or shrimp farming.

There are many techniques to overcome the excessive NH_3–N pollution in the fish farm setting, such as electrocoagulation [8], trickling filtration [9], aerated filtration [10], etc. Due to the complexity and expensive equipment required, they are nearly inaccessible for fish farmer in developing countries. In comparison, adsorption can be a cheap and easy-to-operate answer for the problem. Some studies have reported the use of various adsorbents for NH_3–N uptake, such as biochar [11], zeolite [12], nanosorbent composite [13], etc. But in this research, like *killing two birds with one stone*, we use green algae (*C. Linum*) from the fish farm to prepare a polyurethane film adsorbent. The cationic adsorption performance of *C. Linum* have been reported in several studies [14, 15]. Unfortunately, their application is in a powdered form, leading to a separation difficulty. Therefore, in this study, the green algae are prepared in the form of film, by embedding it with the polyurethane film through a simple catalyst-free isocyanate route.

* Corresponding author.
E-mail address: marlina@unsyiah.ac.id (Marlina).

https://doi.org/10.1016/j.heliyon.2020.e04590
Received 1 May 2020; Received in revised form 14 July 2020; Accepted 28 July 2020

A very intriguing study by Schultz-Jensen et al., (2013) found that a simple dry ball milling method allowed the enzymatic conversion of carbohydrate from *C. Linum* into bioethanol [16]. The study compared five different pretreatments, including wet chemical methods. It revealed ball milling as the best method, not only because it yields the highest bioethanol, but also the lowest biomass weight loss. It is also reported that *C. Linum* is rich in carbohydrate [16, 17], which further suggests the potential use of *C. Linum* as polyol source. Indeed, there are studies reported the use of *C. Linum* as polyol source [18, 19, 20], but they used the oil extracted through complex wet chemical process.

This research is the first to report the preparation of polyurethane film, synthesized from crude *C. Linum* ball-milled particles. The pretreatment cuts the production line, as it does not require the oil extraction. Moreover, cellulosic polyol feed was acquired without involving the hydrolysis, pulping, and bleaching steps [21, 22]. In addition, the ball-milling pretreatment can be considered eco-friendly, as it is free from chemical processing. This research further investigates the potential application of algae-based polyurethane (AlgPU) film in NH_3–N adsorption. *C. Linum* is one of the green algae, in which its rich content of hemicellulose complex (consisted of xylans and mannans) has been suspected to be responsible in the high uptake of heavy metal ions [15].

The adsorption performance would be enhanced by means of activated carbon filler addition. Activated carbon was selected because it was made of biomass, which was the focus of this research in optimizing the biomass-based adsorbent. Previous studies had reported that carbonaceous fillers can modify the material's hydrophilicity, morphology, surface charge, and surface area that of beneficial for pollutant uptake [23, 24, 25]. There are other options such as carbon nanotube and graphene oxide, but to obtain the structure, more complex preparation and chemicals are required [26, 27]. Since the concept of this research is to develop a cheap and easy-to-prepare material, activated carbon is chosen instead. In addition, activated carbon has been reported as an effective adsorbent for wide range of pollutants [28, 29]. Hopefully, the material can be an alternative for fish and shrimp farmers, especially in developing countries.

2. Materials and methods

2.1. Materials

Chemicals and materials used in this research were as follows: 4,4′-methylene diphenyl diisocyanate (MDI), 1,4-dioxane, NH4Cl as feed material for NH_3–N, Nessler's reagent, HCl 0.1 N, NaOH 0.1 N, and distilled water. All of them are analytical grade and, except for distilled water, purchased from Merck. The activated carbon (AC) filler was also analytical grade and purchased from Merck with molar mass of 12.01 g/mol, melting point of 3550 °C, and bulk density of 150–440 kg/m^3.

2.2. Specimen taxonomy profile

Algae specimen was taken from a local fish farm in coastal area of *Gampong* (Village) Deah Raya, Syiah Kuala District, Banda Aceh City, Aceh Province, Indonesia with taxonomy details below:

Regnum/Kingdom: Protista
Phyllum: Chlorophyta
Classic/Class: *Ulvophyceae*
Ordo/Order: *Cladophorales*
Familia/Family: *Cladophoraceae*
Genus/Genus: *Chaetomorpha*
Species/Species: *Chaetomorpha Linum* (O.F. Muller) Kuitzing
Synonym: *Chaetomorpha Crassa* f. tenuior Schiffner

2.3. Ball mill pre-treatment

C. Linum taken from the fish farm was firstly cut into small pieces (±20 mm), repeatedly soaked in the distilled water, and left in the distilled water for another 12 h to remove the impurities [30]. Then, the specimen was rinsed and drained before boiled in distilled water at 100 °C for 15 min, followed by drying process under the sunlight. The dried algae were collected and put in a crusher to obtain crude algae powder (<0.5 mm). Ball milling pre-treatment took place afterward, using Fritsch Pulverisette 7 Premium line, where the crude powder (25 g) was milled in a cylinder with 25 balls (diameter = 15 mm) at 180 rpm for 15 h [16]. The product of this procedure was labeled as algal polyol particle (APP).

2.4. Preparation of algae-based polyurethane film

Algae-based polyurethane (AlgPU) film was mainly prepared by reacting APP as the biopolyol and MDI as the diisocyanate. The polymerization did not require the addition of catalyst since MDI is chemically reactive. APP was weighed as much as 0.5 g, later dissolved in 10 mL dioxane within a beaker glass for 5 min at 500 rpm and room temperature (28 °C) to create a polyol solution. Afterward, MDI was added dropwise to the polyol solution to initiate the formation of PU. MDI volume as much as 3 ml was taken based on our unpublished preliminary research, where the formation of PU was clearly observed through Fourrier Transform – Infrared (FT-IR) analysis and more of that volume lead to high MDI excess. Next, the mixture was left at room temperature and 250 rpm for approximately another 30–45 min. Whilst stirred, AC fillers were added slowly, with weight variation according to Table 1. Since this is a newly developed material, the amounts of AC filler were selected on the basis of trial-and-error. The doping mixture was stirred continuously until it is sufficiently thickened (±15 min). This step of the procedure gave the casting solution, which after that, it was poured onto a glass plate and left until dried at room temperature. The film was cut 1 × 1 cm^2, washed with acetone, and dried in an oven at 70 °C for 12 h.

2.5. Characterization

Identification of the functional groups of AlgPUs was conducted using Shimadzu 8400 Fourrier Transform – Infrared (FTIR). For the surface morphology, JEOL JSM 6510 LA Scanning Electron Microscopy – Electron Dispersive Spectroscopy (SEM-EDS) was employed. The thermal characterization was conducted on Shimadzu DSC-60 Differential Scanning Calorimetry (DSC) (atmosphere: nitrogen (30 ml/min); sample weight: 7g; and temperature: 25–600 °C (15 °C/min.)). Mechanical properties of the samples were obtained from the measurement using Universal Testing Machine HT8503.

The values of specific surface area were calculated from Brunauer-Emmett-Teller (BET), while the values of pore size and pore volume were from Barret-Joyner-Halenda (BJH) using the data of nitrogen adsorption-desorption at 77.3 K on QuadraSorb Station 1 (ver. 5.06). Each sample was priorly degassed at 65 °C for 3 h.

2.6. Batch adsorption

Firstly, the NH_3–N stock solution was prepared by dissolving 3.819 g NH_4Cl, which had been priorly dried in an oven (100 °C; 2 h), with 1,000 ml distilled water in a volumetric flask. Batch adsorption was carried out in an Erlenmeyer 100 ml, filled with 25 ml NH_3–N. As much as 0.035 g AlgPU film (1 × 1 cm^2) was added, then left at room temperature. For contact time effect study, the adsorbent was left for 0–150 min; for pH effect study, the adsorption was set at the equilibrium contact time and pH 4–10; and for concentration effect study, the NH_3–N concentration was varied from 0.05-1.5 ppm. The range of NH_3–N concentration was selected based on the real concentration we obtained from the local fish farm. The concentration of NH_3–N after the adsorption was determined using UV-VIS (Uvmini-1240, Shimadzu), with the help of Nessler's reagent. The results were expressed as adsorption capacity at t time (q_t (μg/g)) or adsorption capacity at equilibrium (q_e (μg/g)) with the equations below:

Table 1. Composition of AlgPUs.

Label	AC filler (g)	APP (g)	MDI (ml)	1,4-Dioxane (ml)
AlgPU	-	0.5	3	10
AC/AlgPU1	0.01	0.5	3	10
AC/AlgPU2	0.03	0.5	3	10

$$q_t = \frac{C_0 - C_t}{W_x} x V_y \quad (1)$$

$$q_e = \frac{C_0 - C_e}{W_x} x V_y \quad (2)$$

Where C_o, C_t, C_e, W_x, and V_y are initial concentration (μg/ml), concentration at t time (μg/ml), concentration at equilibrium (μg/ml), weight of x adsorbent (g), and volume of y adsorbate (ml), respectively.

3. Results and discussion

3.1. Synthesis and infrared spectra of algae-based polyurethanes

Ball milling pre-treatment allows the reduction of particle size, thus can react with MDI to perform a condensation reaction to give a urethane linkage. The reaction with MDI is ascribed to the presence of rich hydroxyl group within the particles. Studies showed that polyurethane can be obtained respectively from cellulose [31], hemicellulose [32], and lignin [33]. As reported by Schultz-Jensen et al. [16] and Zhang et al. [34], the contents of plant cell wall, particularly *Chaetomorpha linum*, are filled with polysaccharides, proteins and pectin. Polysaccharides including the cellulose and hemicellulose complexes, as well as lignin, have more than one OH in its molecule, giving access for the formation of polyurethane (PU) [35]. However, crude powder of *C. linum* did not form a PU film. Only after the ball milling pre-treatment, the film was obtained. This is in agreement with Schultz-Jensen et al [16], where they found the ball-milled algae was more reactive as a consequence of particle size reduction, observed by a highest conversion of biomass into ethanol. Hence, by manipulating the particle size through ball milling, we can make hydroxyl group rich particles, which later called as the algal polyol particle (APP) (Figure 1a).

There are two possibilities on how the reaction between APP and MDI take place (Figure 1b,c). First is a direct reaction, resulting in the embedment of *big* APPs, while second possibility suggests the split up of a big APP into small APPs before forming the urethane polymeric chain. It cannot be determined whether one reaction route is more dominant to the other or not, as the quantitative information is not applicable. The different sizes of APP embedded in Alg/PU can be seen through SEM analysis, which will be discussed later. The reaction can be attributed to the solubility of the APP in 1,4-dioxane, facilitating the split up of big APP. Nevertheless, our recent study found that the MDI also plays a role in the dispersion of APP due to its strong nature of reactivity [35, 36].

The rich content of OH group in the APP can be seen from the FT-IR spectra of APP at a broad spectrum of around 3750–3000 cm^{-1} (Figure 2). The reduction of spectrum width can be assigned to the conversion of hydroxyl group into NCOO, where NH peak is observed clearer. The change is owing to the absence of OH which originally contributes in a strong hydrogen bond, resulting in a broad spectrum consisted of multiple overlapping bands. Bending vibration of NH and OH, observed at around 900-700 cm^{-1}, can also be used to confirm the formation of PU owing to the increase absorbance of NH. On the other hand, stretching bands at around 2250 cm^{-1} is attributed to the excess of MDI. Thus, C=N bands at around 1600 cm^{-1} can be both associated to the excess MDI or the PU formation.

Interestingly, the fingerprint region of algal cellulose can be clearly observed in APP and AlgPU spectra, due to the bending vibration of C–H or stretching vibration of C–O or C–C [37]. Yet, in AC/AlgPU spectrum, the fingerprint region is not so observable, which can be ascribed to the presence electron density disturbance from AC. The aromatic rings of AC, in which many studies had associated them to the adsorption performance, can be observed through the C=C bending bands at around 1500 cm^{-1}. A distinctive band at 1640-1620 cm^{-1}, are assigned to the algal protein (amide I), associated to the C=O stretching motion of the α structures of proteins [32, 33, 34]. A more complex absorbance of collective NH bending and CN stretching is also

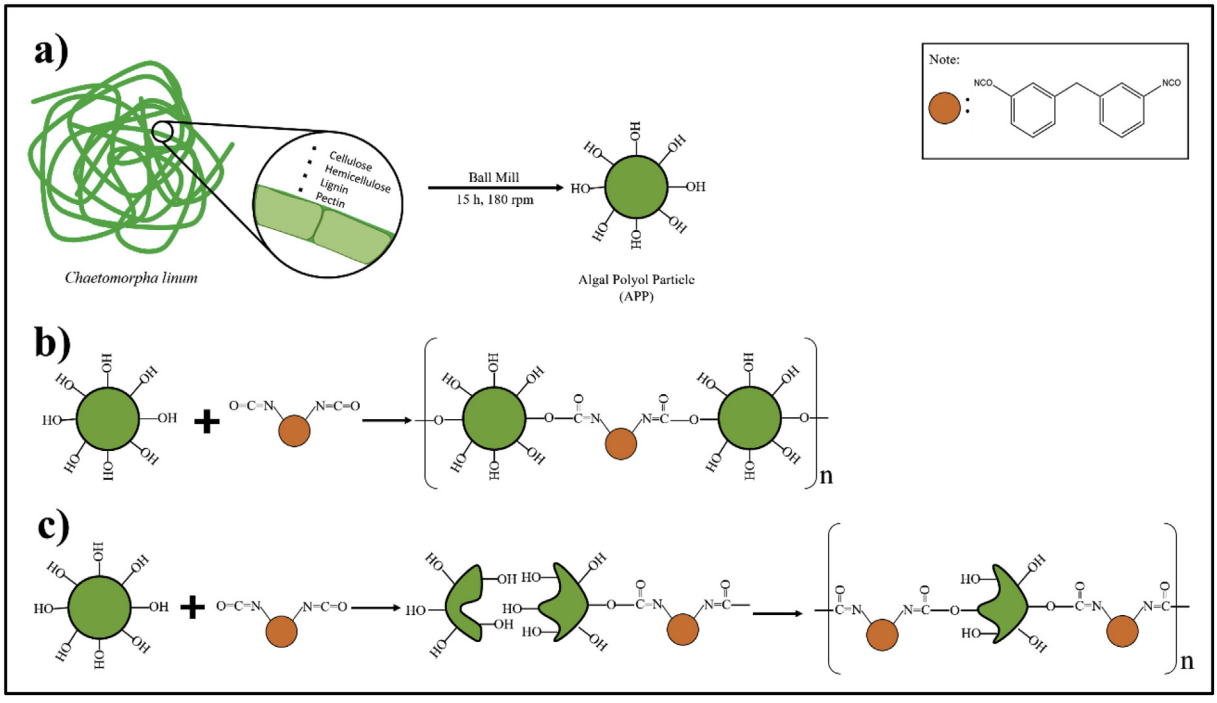

Figure 1. a) The preparation scheme of algal polyol particle (APP); b) the formation of polyurethane from big APP; and c) the polyurethane obtained after the breakup of big app into small APPs.

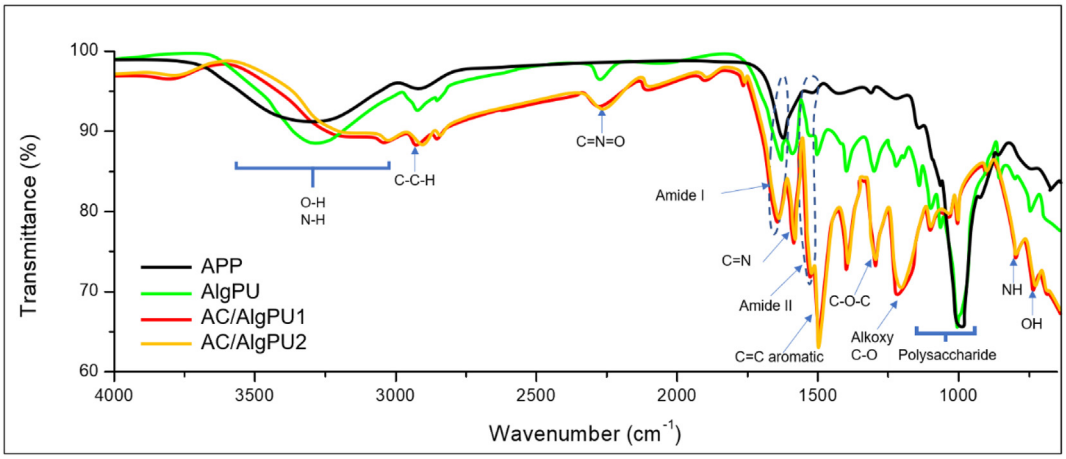

Figure 2. FT-IR spectra of algal polyol particle (APP), algae-based PU (AlgPU), activated carbon filled AlgPU (AC/AlgPU1 and AC/AlgPU2).

observable at 1550-1530 cm^{-1}, which can be assigned to amide II band. The presence of amide I and amide II bands at the FT-IR spectra suggest the presence of protein contents, which is commonly found in plant samples [16, 17, 31, 39].

3.2. Scanning electron microscopy – electron dispersive spectroscopy analysis

APPs, as shown in Figure 3a, have a rough diameter of 5 μm. Salt crystals are also observable in the SEM images, which might be attributed to the origin of the algae. The salt crystals have a distinctive shape compared to the granular particles of APP. Since the specimens were taken from coastal area, the presence of salt contents is understandable. Figure 3b shows the produced AlgPU, where the rectangle-shaped particles are observable, suspected as micro fibrous cellulose particles. It suggests that the cellulose fibers can maintain its form amidst the urethane producing reaction. By comparing the surface (Figure 3b) and cross-section (Figure 3c) of AlgPU, we can see the different layers of this film. The smooth layer is covering the outer layer of the film, meanwhile the supporting layer is found in the cross-section. It has a similarity with membrane structure, suggesting the possible application of this film in membrane filtration.

The presence of granular particles in the cross-section part is more observable than in the surface part. Supposedly, the granular particles is not expected after the polycondensation reaction with MDI. The presence of this granular particles can be associated to the big APP which does not experience a dispersion through multiple break ups. The break up can be ascribed to the solubility of APPs in 1,4-dioxane or the strong attraction of the urethane linkage formed from the reaction with MDI [35, 36]. This phenomenon leads us to the two possible reaction as described previously. Other than big APPs, based on the EDS spectrogram (Figure 3e), the inner part is rich of mineral salts. It is possible that the salt accumulation in the inner part is due to the dense outer layer of polyurethane linkage made of small APPs. This difference of density pushes the less compatible particles (including the big APP), to the inner layer. It also explains the separation of cellulose microfibrils from the APP.

The addition of activated carbon filler results in rougher surface, as can be observed in Figure 3d. Rough surface facilitates adsorption better than smooth surface stem from the increase in contact surface. It also suggests how activated carbon addition cancels the formation of dense layer by blocking the propagation of urethane linkage. This is due to the possession of –OH group in activated carbon reacted with the isocyanate end, yet it preserves the heterogenous phase. It then results in the propagation blockage of the polyurethane. As observed, several activated carbons appear distinctively on the film surface.

3.3. Thermal analysis

Thermal stability of an adsorbent is an important parameter when it comes to its storing and usage conditions. Furthermore, by conducting a thermal analysis, the constituent of the biopolymer complexes within the AlgPUs can be confirmed. Thermal profiles of AlgPU, AC/AlgPU1, and AC/AlgPU2 are presented in a DSC thermogram, as can be seen in Figure 4. The first endothermic peaks at 95 and 105 °C of AC/AlgPU1 and AlgPU, respectively, are assigned to the water evaporation. The lower temperature as well as more negative DSC value, at the said peak, suggest more water absorbed by the AC/AlgPU compared to AlgPU. The second peak (241, 244 and 248 °C for AC/AlgPU2, AC/AlgPU1 and AlgPU, respectively) appears in exothermal form which can be assigned to the decomposition and charring of either hemicellulose and lignin. A study by Yang et al. (2007), which investigated the DSC profiles of respective hemicellulose and lignin, found exothermal peaks assigned to the charring [40]. The charring is specified to be experienced by the hemicellulose and lignin in the big APP, since they are not fully bound to the urethane linkage, resulting in receiving direct thermal impact. Urethane bond cleavage is detected at the following endothermal peak at 264, 273 and 274 °C for AlgPU AC/AlgPU2 and AC/AlgPU1, respectively. The cleavage in both AC/AlgPU1 and AC/AlgPU2 requires higher temperature, indicating the more thermally stable urethane linkage. The improved thermal stability might be ascribed to the addition of activated carbon.

Peaks within 300–500 °C are associated with the multiple degradation of hemicellulose complex constituents. According to a study conducted by Werner et al. (2014), from low to high degradation temperature, the hemicellulose constituents are as follows: Xylan, arabinoxylan, arabinogalactan, galactomannan, glucomannan, xyloglucan, β-glucan and cellulose [41]. Xylan was found to be the only one with consistent exothermal degradation. Thus, the exothermal peak at 331 °C is attributed to xylan's degradation. However, the endothermal peaks exhibited by both AC/AlgPU1 and AC/AlgPU2 at around the same temperature (340 °C) might have overlapped xylan's exothermal peak. The endothermal process can be assigned to the first pyrolysis of activated carbon, where it can also be observed by a very small endothermal peak in AlgPU thermogram right after xylan's degradation. The following peaks (454, 456 and 484 °C for AC/AlgPU1, AC/AlgPU2 and AlgPU, respectively) with negative DSC values are associated for the abscission of functional groups. Last endothermal behaviors of AC/AlgPU1, AC/AlgPU2 and AlgPU are found at 590, 591 and 579 °C, respectively, showing the second pyrolysis. Interestingly, both AC/AlgPU1 and AC/AlgPU2 give more negative DSC value at this peak, which can be ascribed to the AC addition. This is in a good agreement with other studies [42, 43].

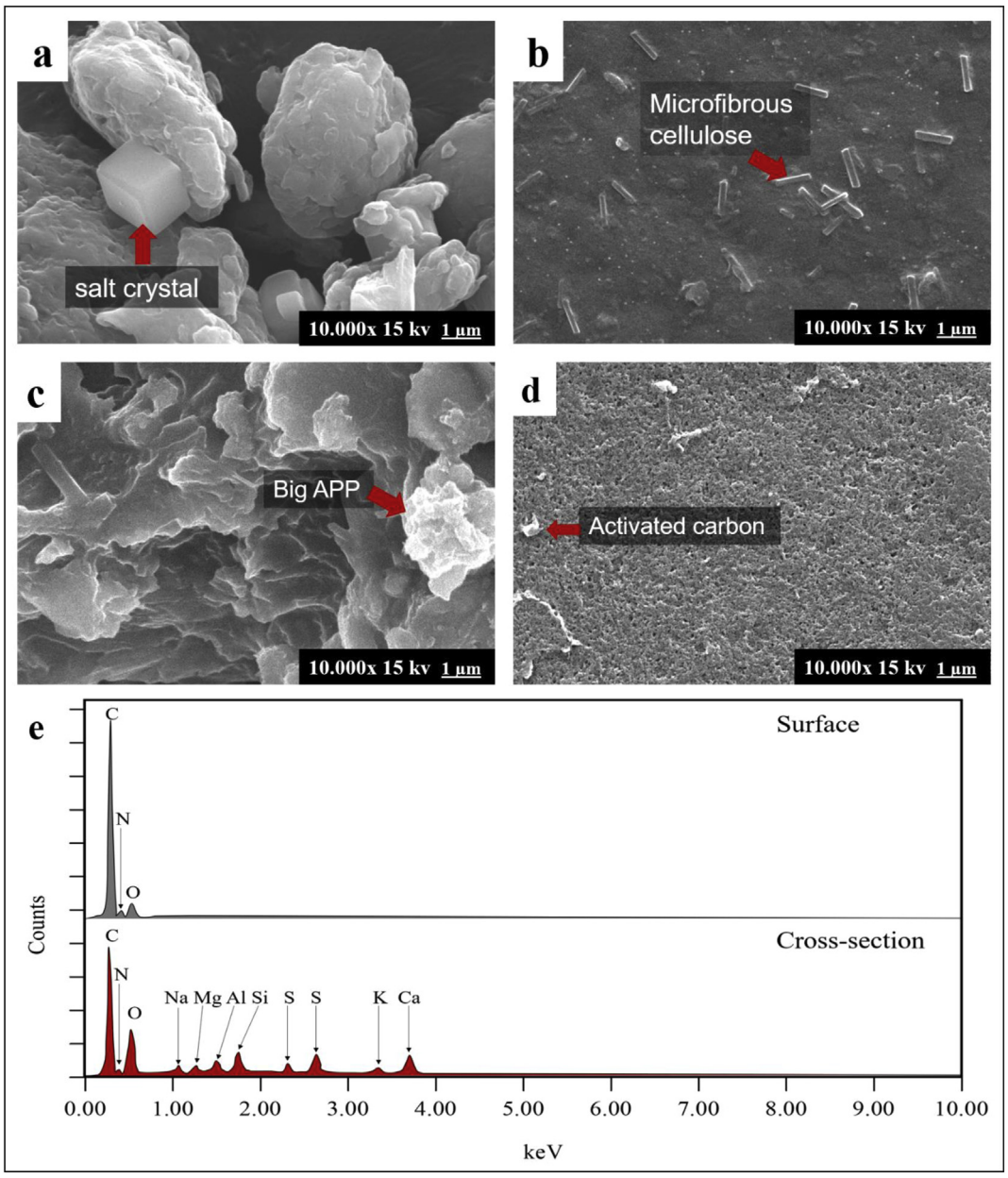

Figure 3. SEM images of a) APP, b) AlgPU surface, c) AlgPU1 cross-section, and d) AC/AlgPU1 surface; and e) EDS spectrogram of AlgPU.

3.4. Mechanical strength profile

Mechanical properties are considering factors when it comes to film-shaped adsorbent. This is owing to the purpose of manufacturing the adsorbent in a film shape is for easy separation and filler immobilization. In its application, an adsorbent material should be mechanically durable against the water pressure. Therefore, the mechanical strength properties of AlgPU, AC/AlgPU1 and AC/AlgPU2 were characterized and presented in Table 2. AC/AlgPU1, which was obtained from the addition of 0.01 g activated carbon, gives much less tensile strength with as high as 75% reduction. Rahmi et al. (2018) [44] and Hosseini et al. [45] correlated this change of mechanical behavior with the interfacial bonding affected by cohesive and adhesive forces. Poor interfacial bonding means there are filler particles blocking the polymer chain formation. In this study, it further leads to the decrease of adhesion between fillers and AC/AlgPU1, which also means the increase in cohesive force. The further decrease was also found on AC/AlgPU2.

It is worth mentioning that, the percentage of activated carbon in AC/AlgPU1 is 6% (w/w). Other studies such as Pei et al. (2018) and Hosseini et al. (2017) reported the decrease of tensile strength after the addition of 1% and >0.05% (w/w) [40, 41]. Thus, no wonder if our material experienced a huge decline in tensile strength after the addition of activated carbon. However, the tensile strengths of AC/AlgPU1 and AC/AlgPU2 are still in par with their materials, especially Hosseini et al. (2017) in which their material only reached 3.65 MPa at maximum [45]. Even though the mechanical properties of AlgPU1 and AC/AlgPU2 are worse than AlgPU, including the 45–48% reduction of elongation at break, the adsorption ability is far off better, which will be explained in the following section.

3.5. Adsorption

3.5.1. Effect of contact time and filler

The initial phase of adsorption is mostly governed by the diffusion of adsorbate carried by water onto the adsorbent surface. As can be seen in

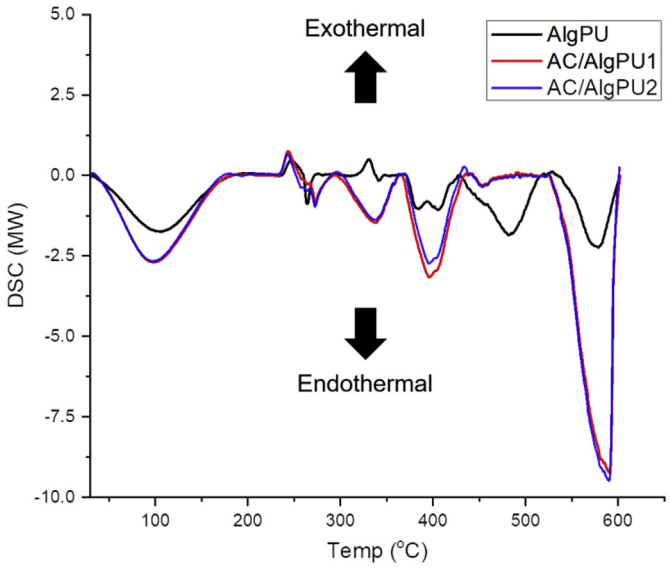

Figure 4. DSC thermogram of AlgPU, AC/AlgPU1 and AC/AlgPU2 films.

Table 2. Mechanical properties of AlgPU and AC/AlgPU1.

Sample	Tensile Strength (MPa)	Elongation %
AlgPU	59.92	5.46
AC/AlgPU1	15.20	2.98
AC/AlgPU2	13.96	2.83

Figure 5a, the adsorption capacities of NH_3–N at the first 30 min for all adsorbents (AlgPU, AC/AlgPU1, and AC/AlgPU2) increase rapidly, suggesting the diffusion dominated phase. NH_3–N adsorption on AC/AlgPU1 show an immediate and the highest increase at the first 10 min. The rougher surface morphology (as captured in the SEM image), may have a role in facilitating the diffusion. It is corroborated by the surface area and pore size of the respective materials, as can be seen in Table 3. The addition of filler increased the surface area and provided higher quantity of pores, as reported previously [23].

AC/AlgPU2, however, starts at a lower adsorption capacity, which is similar to our previous report [47]. The increase of filler addition may have an effect on its structure; elevating the density and closing the pores. It is further explained by the decrease in surface area and pore volume of AC/AlgPU2. Nevertheless, the surface area was not the only responsible factor for the adsorption. It is due to the fact that although the AC/AlgPU2 had a lower surface area, the adsorption capacity was still higher than AlgPU. It can be ascribed by the higher availability of functional groups from activated carbon fillers. The significance of functional groups in the adsorption has been acknowledged by other studies [44, 48].

For the next 90 min, the NH_3–N adsorption is driven by the intermolecular interaction, such as electrostatic attraction, hydrogen bond, Van der Waals interaction, etc. The equilibrium is reached at 120 min as the adsorption capacities of all adsorbents stop increasing. Thus, adsorption performance of each adsorbent is compared at 120 min and presented in Figure 5b. AlgPU has the adsorption capacity of 187.84 μg/g, and it increases to 393.43 μg/g after the addition of 6% (w/w) activated carbon. Some studies had reported the use of algae as biosorbent, where the pollutant uptake occurred through physical or chemical adsorption [14, 15]. AlgPU has a variety of active sites that could interact with the adsorbate, especially due to the constituents of its algal cell wall

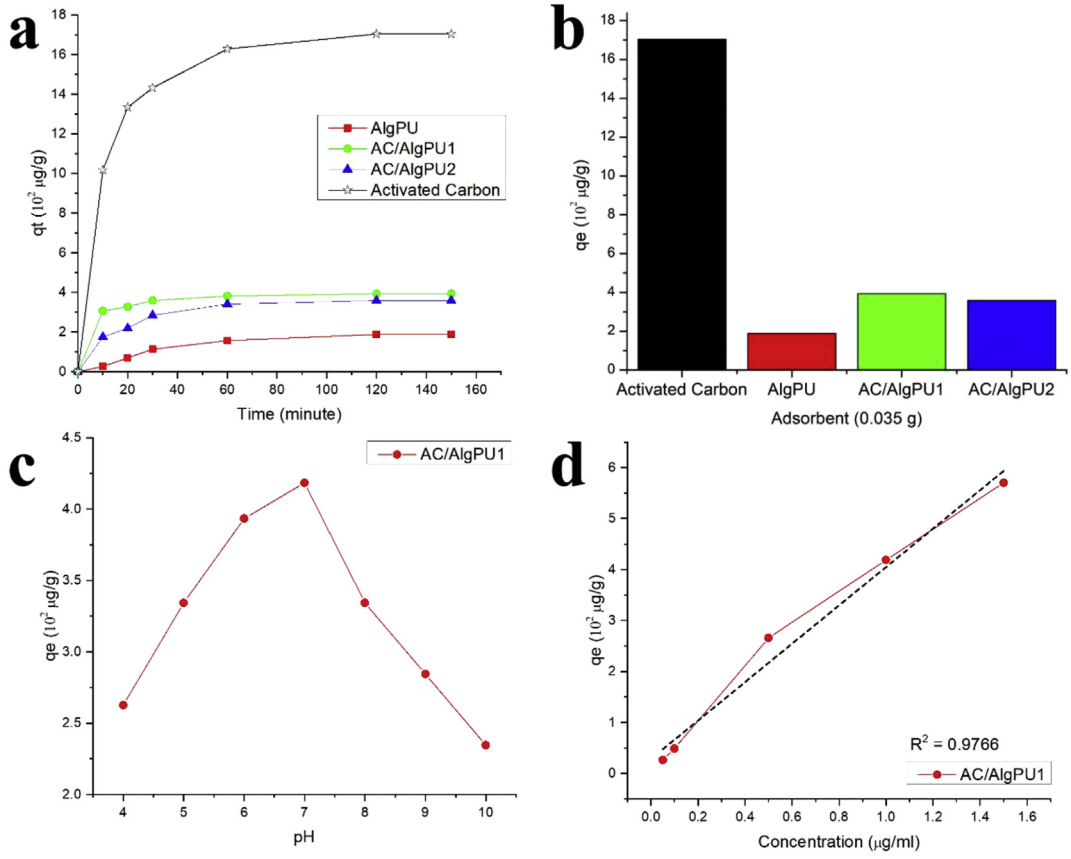

Figure 5. a) effect of contact time of AlgPU, AC/AlgPU1, and AC/AlgPU2; b) comparison of 0.035 g activated carbon (AC), AlgPU, AC/AlgPU1, and AC/AlgPU2 adsorbents; c) effect of pH; and d). effect of concentration.

Table 3. Surface area, pore size, and pore volume.

Sample	Surface area (m^2/g)	Pore size (nm)	Pore volume (cm^3/g)
AlgPU	33.446	1.676	0.026
AC/AlgPU1	47.678	1.696	0.037
AC/AlgPU2	29.815	1.677	0.024

(cellulose, hemicellulose, lignin). Therefore, the ability to adsorb NH_3–N on the AC/AlgPUs comes from the attraction combination of activated carbon and AlgPU.

Nevertheless, neat activated carbon gives the highest adsorption capacity (1704.10 μg/g). It can be explained by the small size of powdered activated carbon, contributing to higher contact surface area. Furthermore, activated carbon adds more functional groups, observed by the increase in absorbance intensity of the FT-IR spectra, in which it can be attributed to a higher number of binding sites [35]. This fact is in line with the previous reported studies, by comparing the Cu (II) adsorption on raw *C. Linum* [15] with that of on the activated carbon prepared from hazelnut husk, where the adsorption was higher on the prepared activated carbon [49]. However, the application of granular adsorbents is limited by its separation difficulty [46]. Film adsorbent, on contrary, can be easily removed from the water, resulting in less requirement for the separation equipment in the water treatment system. In addition, the activated carbon content in 0.035 g AC/AlgPU1 is only 0.002 g, which is 17.5 times less than 0.035 g neat activated carbon, yet it still can carry more than a fifth of neat activated carbon adsorption capacity. Therefore, less amount of activated carbon is required when combined with AlgPU matrix. It suggests that the AlgPU film is a good material to immobilize the activated carbon filler.

3.5.2. Effect of pH

One of the important parameters in adsorption is pH, because the adsorption capacity can be affected with the change of pH (see in Figure 5c). The optimum NH_3–N uptake was obtained when the initial pH is adjusted to 7. The adsorption capacity changed slightly at lower pH (6) and dropped greatly at higher pH (8). The value obtained for pH Point Zero Charge (pH_{pzc}) of AC/AlgPU2 was 6.59, in which below that point, the surface has a positive charge. This value of pH_{pzc} was obtained through pH drift method as conducted by Park et al [11].

The pH_{pzc} explains the lower adsorption capacity when the pH of the adsorbate solution is below 7. Within acidic pH range, NH_3–N maintains its cationic form (NH_4^+). Due to the same positive charge of the adsorbent and adsorbate, the repulsive force is expected from the electrostatic interaction. Moreover, under pH 7, the presence of competing cations (H^+) is significant. Meanwhile, when the pH is below 7, the NH_3 is more dominant, making the electrostatic attraction cannot take place. The optimum adsorption is observed at pH 7 owing to the electrostatic attraction between the adsorbate and adsorbent having the opposite surface charges. Since pH 7 give the best adsorption capacity, it is then selected as the optimum pH and used for the rest of the study.

3.5.3. Effect of concentration

Figure 5d shows the effect of concentration on NH_3–N adsorption onto AC/AlgPU1. The adsorption capacity increases, as the initial NH_3–N concentration increases forming a linear curve with coefficient of determination (R^2) = 0.9766. It is due to the fact that more NH_3–N present in the solution gives a higher force diffusing the pollutant solution onto the solid surface of the adsorbent. Park et al., [11] found that the change of adsorption capacity is not proportional with the adsorbent dosage increase. Therefore, in this study, the variation of concentration is used for the following isotherm studies.

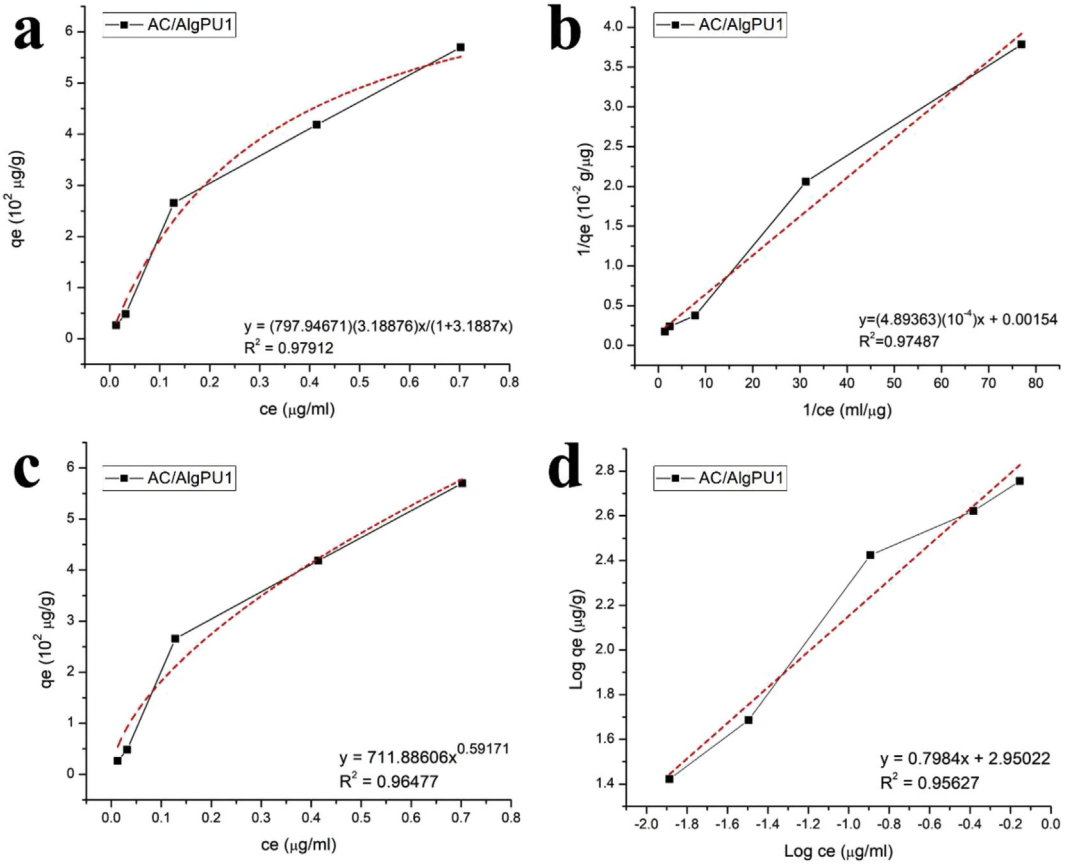

Figure 6. a) non-linear and b) linear curves of Langmuir isotherm; and c) non-linear and d) linear curves of Freundlich isotherm.

Table 4. Types, equations, and constant values of Langmuir and Freundlich isotherm model.

Isotherm Model	Type	Equation	Obtained values	
Langmuir	Non-linear	$q_e = \frac{Q_m K_L C_e}{1 + K_L C_e}$	Q_m	797.95
			K_L	3.19
			R^2	0.97912
			RMSE	33.91952
	Linear	$\frac{1}{q_e} = \frac{1}{Q_m} + \frac{1}{K_L Q_m C_e}$	Q_m	649.35
			K_L	3.15
			R^2	0.97487
Freundlich	Non-linear	$q_e = K_F C_e^{\frac{1}{n}}$	K_F	711.89
			$1/n$	0.59
			R^2	0.96477
			RMSE	44.05388
	Linear	$Log\ q_e = Log\ K_F + \frac{1}{n} LogCe$	K_F	891.70
			$1/n$	0.80
			R^2	0.95627

Note: Q_m is maximum monolayer coverage capacities (μg/g); K_L is Langmuir isotherm constant (l/μg); K_F is Freundlich isotherm constant related to adsorption capacity ((μg/g) (ml/g)); and n is adsorption intensity.

3.6. Isotherm studies

This isotherm study aims to comprehend the behavior of NH_3–N adsorption onto AC/AlgPU1. Langmuir isotherm model uses the assumption that the adsorption occurs in monolayer with each binding site has homogenous energy. The isotherm model also assumes the absence of interaction between the adsorbates. On contrary, Freundlich isotherm model is based on the assumption that the adsorption is multilayers, where the binding energy is different at each active site. Isotherm models can be used to provide an estimation for the adsorption by constructing the estimated line (the red dashed-line) for each isotherm model curve (Figure 6). The equation along with the obtained constant values for each type of the isotherm models can further be seen in Table 4.

The value of R^2 can be used to determine the fitness between the experimental data (black solid-line) and the data estimated from isotherm model. R^2 for non-linear and linear Langmuir isotherm model respectively are 0.97912 and 0.97487, meanwhile for non-linear and linear Freundlich isotherm model the R^2 respectively are 0.96477 and 0.95627. Firstly, the R^2 in non-linear isotherm model is indistinctively bigger than the linear one. This is in agreement with several reported studies, pointing out the non-linear isotherm is more accurate [50]. It is owing to the fact that the linear equation is derived from the non-linear one, where in the process, some information might have gone missing. In addition, Heydari et al. [51] had proposed a nonlinear optimization for enzyme kinetics and found a good accuracy of the method.

The comparison between R^2 values further suggest that NH_3–N follows the assumption in the Langmuir isotherm model, having a monolayer and homogenous adsorption. The adsorption dependence on Langmuir isotherm model is substantiated by the lower *root-mean-square error* (33.91952), compared to the one obtained from the Freundlich isotherm model (44.05388). As can be seen in Table 4, the estimated maximum adsorption capacity (Q_m) is as high as 797.95 μg/g. This value is greater compared to the biomass-based adsorbents prepared by Abuabdou et al. [52] and Erabee et al. [53], which gave 50.8 and 45.4 μg/g, respectively. Yet, AC/AlgPU still need to be improved to achieve higher maximum adsorption capacity as reported by many other studies [54, 55].

4. Conclusion

This study had achieved a simple preparation method using ball mill pre-treatment to obtain a new algae-based polyurethane (AlgPU) film adsorbent, and further filled with activated carbon. Two reaction pathways had been proposed based on FT-IR and SEM-EDS analysis. The reaction was made possible due to the particle reduction of *C. Linum* using ball milling method. The effect of activated carbon filler addition was observed to give beneficial properties, such as rougher surface and more thermal stability, but not in tensile strength. Activated carbon filler greatly improved the adsorption capacity by 109.45%. This improvement was attributed to the contribution of activated carbon in giving more functional group and larger surface area. The investigation on pH effect revealed the adsorption was governed by the electrostatic attraction and NH_3–N species in aqueous system. The NH_3–N adsorption onto AC/AlgPU1 was Langmuir isotherm model dependent, suggesting the monolayer adsorption with homogenous energy at each binding sites. We recommend further research on using bio-based or less toxic isocyanate to increase the eco-friendliness of the material.

Declarations

Author contribution statement

Marlina: Conceived and designed the experiments; Contributed reagents, materials, analysis tools or data; Wrote the paper.

Muhammad Iqhrammullah: Performed the experiments; Wrote the paper.

Sitti Saleha: Conceived and designed the experiments; Contributed reagents, materials, analysis tools or data.

Fathurrahmi: Analyzed and interpreted the data; Contributed reagents, materials, analysis tools or data.

Fandini Putri Maulina: Performed the experiments.

Rinaldi Idroes: Analyzed and interpreted the data.

Funding statement

This work was supported by the Universitas Syiah Kuala through Penelitian Unggulan Unsyiah (PUU) scheme [278/UN11.2/PP/PNBP/SP3/2019].

Competing interest statement

The authors declare no conflict of interest.

Additional information

No additional information is available for this paper.

Acknowledgements

The authors appreciate the assistance from Department of Chemistry, Faculty of Mathematics and Natural Sciences, Universitas Syiah Kuala.

References

[1] D. Halim, Juanri, Indonesia's aquaculture industry, 2016.
[2] S.A. El-Shafai, F.A. El-Gohary, F.A. Nasr, N.P. van der Steen, H.J. Gijzen, Chronic ammonia toxicity to duckweed-fed tilapia (Oreochromis niloticus), Aquaculture 232 (2004) 117–127.
[3] H.-J. Wang, X.-C. Xiao, H.-Z. Wang, Y. Li, Q. Yu, X.-M. Liang, W.-S. Feng, J.-C. Shao, M. Rybicki, D. Jungmann, E. Jeppesen, Effects of high ammonia concentrations on three cyprinid fish: acute and whole-ecosystem chronic tests, Sci. Total Environ. 598 (2017) 900–909.
[4] I.S. Racotta, R. Hernández-Herrera, Metabolic responses of the white shrimp, Penaeus vannamei, to ambient ammonia, Comp. Biochem. Physiol. Part A Mol. Integr. Physiol. 125 (2000) 437–443.
[5] E. Li, L. Chen, C. Zeng, X. Chen, N. Yu, Q. Lai, J.G. Qin, Growth, body composition, respiration and ambient ammonia nitrogen tolerance of the juvenile white shrimp, Litopenaeus vannamei, at different salinities, Aquaculture 265 (2007) 385–390.
[6] C.G.J. van Bussel, J.P. Schroeder, S. Wuertz, C. Schulz, The chronic effect of nitrate on production performance and health status of juvenile turbot (Psetta maxima), Aquaculture 326–329 (2012) 163–167.

[7] E.A. Seymour, The effects and control of algal blooms in fish ponds, Aquaculture 19 (1980) 55–74.

[8] J.N. Hakizimana, B. Gourich, M. Chafi, Y. Stiriba, C. Vial, P. Drogui, J. Naja, Electrocoagulation process in water treatment: a review of electrocoagulation modeling approaches, Desalination (2017).

[9] P. Oyarzun, L. Alarcón, G. Calabriano, J. Bejarano, D. Nuñez, N. Ruiz-Tagle, H. Urrutia, Trickling filter technology for biotreatment of nitrogenous compounds emitted in exhaust gases from fishmeal plants, J. Environ. Manag. 232 (2019) 165–170.

[10] H. Abu Hasan, S.R. Sheikh Abdullah, S.K. Kamarudin, N. Tan Kofli, On–off control of aeration time in the simultaneous removal of ammonia and manganese using a biological aerated filter system, Process Saf. Environ. Protect. 91 (2013) 415–422.

[11] M.H. Park, S. Jeong, J.Y. Kim, Adsorption of NH3-N onto rice straw-derived biochar, J. Environ. Chem. Eng. 7 (2019) 103039.

[12] M. Wang, R. Xie, Y. Chen, X. Pu, W. Jiang, L. Yao, A novel mesoporous zeolite-activated carbon composite as an effective adsorbent for removal of ammonia-nitrogen and methylene blue from aqueous solution, Bioresour. Technol. 268 (2018) 726–732.

[13] S. Wongcharee, V. Aravinthan, L. Erdei, Removal of natural organic matter and ammonia from dam water by enhanced coagulation combined with adsorption on powdered composite nano-adsorbent, Environ. Technol. Innov. 17 (2020) 100557.

[14] R. Foroutan, H. Esmaeili, M. Abbasi, M. Rezakazemi, M. Mesbah, Adsorption behavior of Cu(II) and Co(II) using chemically modified marine algae, Environ. Technol. 39 (2018) 2792–2800.

[15] L.C. Ajjabi, L. Chouba, Biosorption of Cu2+ and Zn2+ from aqueous solutions by dried marine green macroalga Chaetomorpha linum, J. Environ. Manag. 90 (2009) 3485–3489.

[16] N. Schultz-Jensen, A. Thygesen, F. Leipold, S.T. Thomsen, C. Roslander, H. Lilholt, A.B. Bjerre, Pretreatment of the macroalgae Chaetomorpha linum for the production of bioethanol – comparison of five pretreatment technologies, Bioresour. Technol. 140 (2013) 36–42.

[17] D.S. Domozych, M. Ciancia, J.U. Fangel, M.D. Mikkelsen, P. Ulvskov, W.G.T. Willats, The cell walls of green algae: a journey through evolution and diversity, Front. Plant Sci. 3 (2012).

[18] M.S. Pawar, A.S. Kadam, B.S. Dawane, O.S. Yemul, Synthesis and characterization of rigid polyurethane foams from algae oil using biobased chain extenders, Polym. Bull. 73 (2016) 727–741.

[19] C.K. Patil, H.D. Jirimali, J.S. Paradeshi, B.L. Chaudhari, P.K. Alagi, S.C. Hong, V.V. Gite, Synthesis of biobased polyols using algae oil for multifunctional polyurethane coatings, Green Mater. 6 (2018) 165–177.

[20] Z.S. Petrović, X. Wan, O. Bilić, A. Zlatanić, J. Hong, I. Javni, M. Ionescu, J. Milić, D. Degruson, Polyols and polyurethanes from crude algal oil, J. Am. Oil Chem. Soc. 90 (2013) 1073–1078.

[21] D. Hermawan, T.K. Lai, S. Jafarzadeh, D.A. Gopakumar, M. Hasan, F.A.T. Owolabi, N.A. Sri Aprilia, S. Rizal, H.P.S. Abdul Khalil, Development of seaweed-based bamboo microcrystalline cellulose films intended for sustainable food packaging applications, Bioresour 14 (No 2) (2019). https://ojs.cnr.ncsu.edu/index.php/BioRes/article/view/BioRes_14_2_3389_Hermawan_Seaweed_Based_Bamboo_Microcrystalline.

[22] N. Az-Zahra, R. Rahmi, S. Lubis, Reinforcement of chitosan film using cellulose isolated from grass (imperata cylindrica), J. Phys. Conf. Ser. 1402 (2019), 055039.

[23] P. Ghasemipour, M. Fattahi, B. Rasekh, F. Yazdian, Developing the ternary ZnO doped MoS2 nanostructures grafted on CNT and reduced graphene oxide (RGO) for photocatalytic degradation of aniline, Sci. Rep. 10 (2020) 4414.

[24] M. Iqhrammullah, Marlina, R. Hedwig, I. Karnadi, K.H. Kurniawan, N.G. Olaiya, M.K. Mohamad Haafiz, H.P.S. Abdul Khalil, S.N. Abdulmadjid, Filler-Modified Castor oil-based polyurethane foam for the removal of aqueous heavy metals detected using laser-induced breakdown spectroscopy (LIBS) technique, Polymers (Basel) 12 (2020) 903.

[25] P. Tavakoli, S.R. Shadizadeh, F. Hayati, M. Fattahi, Effects of synthesized nanoparticles and Henna-Tragacanth solutions on oil/water interfacial tension: nanofluids stability considerations, Petroleum (2020).

[26] J. Song, X. Wang, C.-T. Chang, Preparation and characterization of graphene oxide, J. Nanomater. 2014 (2014) 1–6.

[27] D. Zhang, L. Shi, J. Fang, X. Li, K. Dai, Preparation and modification of carbon nanotubes, Mater. Lett. 59 (2005) 4044–4047.

[28] C. Souza, D. Majuste, M.S.S. Dantas, V.S.T. Ciminelli, Effect of zinc ion on copper speciation and adsorption on activated carbon, Hydrometallurgy 176 (2018) 78–86.

[29] G.Z. Kyzas, G. Bomis, R.I. Kosheleva, E.K. Efthimiadou, E.P. Favvas, M. Kostoglou, A.C. Mitropoulos, Nanobubbles effect on heavy metal ions adsorption by activated carbon, Chem. Eng. J. 356 (2019) 91–97.

[30] A. Kłos, M. Rajfur, Influence of hydrogen cations on kinetics and equilibria of heavy-metal sorption by algae—sorption of copper cations by the alga Palmaria palmata (Linnaeus) Weber & Mohr (Rhodophyta), J. Appl. Phycol. 25 (2013) 1387–1394.

[31] H.-J. Hong, J.S. Lim, J.Y. Hwang, M. Kim, H.S. Jeong, M.S. Park, Carboxymethlyated cellulose nanofibrils(CMCNFs) embedded in polyurethane foam as a modular adsorbent of heavy metal ions, Carbohydr. Polym. 195 (2018) 136–142.

[32] G.P. Otto, M.P. Moisés, G. Carvalho, A.W. Rinaldi, J.C. Garcia, E. Radovanovic, S.L. Fávaro, Mechanical properties of a polyurethane hybrid composite with natural lignocellulosic fibers, Compos. B Eng. 110 (2017) 459–465.

[33] O.S.H. Santos, M. Coelho da Silva, V.R. Silva, W.N. Mussel, M.I. Yoshida, Polyurethane foam impregnated with lignin as a filler for the removal of crude oil from contaminated water, J. Hazard Mater. 324 (2017) 406–413.

[34] X. Zhang, W. Yang, W. Blasiak, Modeling study of woody biomass: interactions of cellulose, hemicellulose, and lignin, Energy Fuel. 25 (2011) 4786–4795.

[35] M. Iqhrammullah, M. Marlina, H.P.S.A. Khalil, K.H. Kurniawan, H. Suyanto, R. Hedwig, I. Karnadi, N.G. Olaiya, C.K. Abdullah, S.N. Abdulmadjid, Characterization and performance evaluation of cellulose acetate–polyurethane film for lead II ion removal, Polymers (Basel) 12 (2020) 1317.

[36] M. Iqhrammullah, Marlina, S. Nur, Adsorption behaviour of hazardous dye (methyl orange) on cellulose-acetate polyurethane sheets, IOP Conf. Ser. Mater. Sci. Eng. 845 (2020), 012035.

[37] A. Ertani, O. Francioso, E. Ferrari, M. Schiavon, S. Nardi, Spectroscopic-chemical fingerprint and biostimulant activity of a protein-based product in solid form, Molecules 23 (2018) 1031.

[39] D.G. Ivanova, B.R. Singh, Nondestructive FTIR monitoring of leaf senescence and elicitin-induced changes in plant leaves, Biopolymers 72 (2003) 79–85.

[40] H. Yang, R. Yan, H. Chen, D.H. Lee, C. Zheng, Characteristics of hemicellulose, cellulose and lignin pyrolysis, Fuel 86 (2007) 1781–1788.

[41] K. Werner, L. Pommer, M. Broström, Thermal decomposition of hemicelluloses, J. Anal. Appl. Pyrolysis 110 (2014) 130–137.

[42] M.F. de Salgado, A.M. Abioye, M.M. Junoh, J.A.P. Santos, F.N. Ani, Preparation of activated carbon from babassu endocarpunder microwave radiation by physical activation, IOP Conf. Ser. Earth Environ. Sci. 105 (2018), 012116.

[43] A. Bazan, P. Nowicki, P. Półrolniczak, R. Pietrzak, Thermal analysis of activated carbon obtained from residue after supercritical extraction of hops, J. Therm. Anal. Calorim. 125 (2016) 1199–1204.

[44] Lelifajri Rahmi, R. Nurfatimah, Preparation of polyethylene glycol diglycidyl ether (PEDGE) crosslinked chitosan/activated carbon composite film for Cd2+ removal, Carbohydr. Polym. 199 (2018) 499–505.

[45] S.M. Hosseini, S.H. Amini, A.R. Khodabakhshi, E. Bagheripour, B. Van der Bruggen, Activated carbon nanoparticles entrapped mixed matrix polyethersulfone based nanofiltration membrane for sulfate and copper removal from water, J. Taiwan Inst. Chem. Eng. 82 (2018) 169–178.

[46] Y. Pei, X. Wu, G. Xu, M. Chen, Z. Zhang, X. Zheng, J. Liu, K. Tang, Activated carbon-entrapped microfibrilated cellulose films as an effective adsorbent for removing organic dye from aqueous effluent, J. Wood Chem. Technol. 38 (2018) 15–27.

[47] M. Marlina, Iqhrammullah, Darmadi, I. Mustafa, Rahmi, The application of chitosan modified polyurethane foam adsorbent, RASĀYAN J. Chem. 12 (2019) 494–501.

[48] L. Zhou, Q. Yu, Y. Cui, F. Xie, W. Li, Y. Li, M. Chen, Adsorption properties of activated carbon from reed with a high adsorption capacity, Ecol. Eng. 102 (2017) 443–450.

[49] M. Imamoglu, A. Ozturk, Ş. Aydın, A. Manzak, A. Gündoğdu, C. Duran, Adsorption of Cu(II) ions from aqueous solution by hazelnut husk activated carbon prepared with potassium acetate, J. Dispersion Sci. Technol. 39 (2018) 1144–1148.

[50] K.Y. Foo, B.H. Hameed, Insights into the modeling of adsorption isotherm systems, Chem. Eng. J. 156 (2010) 2–10.

[51] A. Heydari, M. Fattahi, F. Khorasheh, A new nonlinear optimization method for parameter estimation in enzyme kinetics, energy sources, Part A recover, Util. Environ. Eff. 37 (2015) 1275–1281.

[52] S.M.A. Abuabdou, O.W. Teng, M.J.K. Bashir, N.C. Aun, S. Sethupathi, L.M. Pratt, Treatment of tropical stabilized landfill leachate using palm oil fuel ash: isothermal and kinetic studies, Desalin. WATER Treat. 144 (2019) 201–210.

[53] I.K. Erabee, A. Ahsan, B. Jose, M.M.A. Aziz, A.W.M. Ng, S. Idrus, N.N.N. Daud, Adsorptive treatment of landfill leachate using activated carbon modified with three different methods, KSCE J. Civ. Eng. 22 (2018) 1083–1095.

[54] F. Al-Sheikh, C. Moralejo, M. Pritzker, W.A. Anderson, A. Elkamel, Batch adsorption study of ammonia removal from synthetic/real wastewater using ion exchange resins and zeolites, Separ. Sci. Technol. (2020) 1–12.

[55] U. Oyeagu, C. Nwuche, C. Ogbonna, J. Ogbonna, Addition of fillers to sodium alginate solution improves stability and immobilization capacity of the resulting calcium alginate beads, Iran, J. Biotechnol. 16 (2018) 67–73.